Journal of Molecular Graphics and Modelling 46 (2013) 65–73

Contents lists available at ScienceDirect

Journal of Molecular Graphics and Modelling

journal homepage: www.elsevier.com/locate/JMGM

Insight into the mechanism of aminomutase reaction: A case study of phenylalanine aminomutase by computational approach

Kang Wang[a,1], Qianqian Hou[a,1], Yongjun Liu[a,b,*]

[a] Key Laboratory of Theoretical and Computational Chemistry in Universities of Shandong, School of Chemistry and Chemical Engineering, Shandong University, Jinan, Shandong 250100, China
[b] Northwest Institute of Plateau Biology, Chinese Academy of Sciences, Xining, Qinghai 810001, China

ARTICLE INFO

Article history:
Received 27 May 2013
Received in revised form 28 August 2013
Accepted 25 September 2013
Available online 4 October 2013

Keywords:
Aminomutase
Density functional calculations
Enzymatic reaction mechanisms
Phenylalanine aminomutase
Stereochemistry

ABSTRACT

The *Taxus canadensis* phenylalanine aminomutase (*Tc*PAM) catalyze the isomerization of (S)-α-phenylalanine to the (R)-β-isomer. The active site of *Tc*PAM contains the signature 5-methylene-3,5-dihydroimidazol-4-one (MIO) prosthesis, observed in the ammonia lyase class of enzymes. Up to now, there are two plausible mechanisms for these MIO-dependent enzymes, i.e., the amino-MIO adduct mechanism and the Friedel–Crafts-type reaction mechanism. In response to this mechanistic uncertainty, the phenylalanine aminomutase mechanism was investigated by using density functional methods. The calculation results indicate that: (1) the reaction prefers the amino-MIO adduct mechanism where the 2,3-amine shift process contains six elementary steps; (2) the ammonia elimination step proceeds through an E2 mechanism; (3) a single C1—Cα bond rotation of 180° in the cinnamate skeleton occurs in the active site prior to the rebinding of NH_2 group to the cinnamate. This can be used to explain the stereochemistry of the *Tc*PAM reaction product which is contrary to those of the *Pa*PAM and *Sg*TAM enzymes. Based on these calculations, the roles of important residues in the active site were also elucidated.

1. Introduction

β-amino acids are important building blocks of biopolymers and functional molecules, and the preparation of optically pure β-amino acids have received increasing attention in the past decade [1–5]. Recently, notable progress in the development of chemical methods for the synthesis of β-amino acids by using chiral pool approach [6] and asymmetric protocols [7–10] has been achieved. However, biocatalytic routes toward β-amino acids are still very limited due to the narrow substrate range and strict regioselectivity of enzyme-catalyzed reactions. Aminomutases typically catalyze the isomerization of α-amino acids to β-amino acids, providing an alternative synthetic strategy for the preparation of chiral β-amino acids. Aminomutases are usually found in the biosynthetic pathways of biologically active natural products such as blasticidin S [3], enediyne C-1027 [11], viomycin [12] and Taxol [13]. Up to now, about ten aminomutases have been identified, and the stereochemical courses of lysine-2,3- [14,15], tyrosine-2,3- [16,17], arginine-2,3- [3] and β-lysine-5,6-aminomutases [18] reaction have been recognized.

Although these aminomutases catalyze the conversion of α-amino acids to β-amino acids, they exhibit different reaction mechanisms and cofactor dependency. For example, β-lysine-5,6- [18], α-ornithine-4,5- [19], and α-lysine-2,3-aminomutases [14,15] follow the radical-initiated intermediates, and each enzyme employs adenosylcobalamin or S-adenosylmethionine and pyridoxal phosphate as cofactors, whereas tyrosine aminomutase (TAM) [3] from *Bacillus* requires only ATP as a cosubstrate, and its functionally similar orthologue from *Streptomyces* requires no cofactors. A recently discovered enzyme, phenylalanine aminomutases (PAMs), that catalyze the isomerization of (S)-α-phenylalanine to (S)- or (R)-β-phenylalanine, also requires no cofactors (Scheme 1). An interesting aspect of PAM is that its product is an essential biosynthetic precursor of the phenylisoserine side chain of the antimitotic pharmaceutical Taxol [20–22].

Experimental studies have showed that the stereochemistry of PAM is uncommon compared to the above described radical-initiated aminomutase mechanism. For example, when (2S)-α-lysine and (2S)-α-arginine were used as substrates, the corresponding (3S)-β-lysine and (3S)-β-arginine were finally obtained. Further, although *Tc*PAM and *Sg*TAM are both aryl amino acid aminomutases and share the same cofactor dependency and similarity (30% amino acid identity), their stereochemistries are completely different [23–26]; *Sg*TAM catalyze the isomerization

* Corresponding author at: Key Laboratory of Theoretical and Computational Chemistry in Universities of Shandong, School of Chemistry and Chemical Engineering, Shandong University, Jinan, Shandong 250100, China. Tel.: +86 531 88365536; fax: +86 531 88564464.
E-mail address: yongjunliu_1@sdu.edu.cn (Y. Liu).
[1] These authors are contributed equally to this work.

1093-3263/$ – see front matter © 2013 Elsevier Inc. All rights reserved.
http://dx.doi.org/10.1016/j.jmgm.2013.09.010

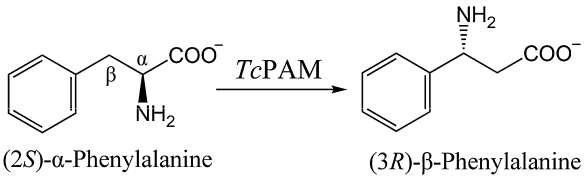

Scheme 1. Isomerization of (2*S*)-β-phenylalanine to (3*R*)-α-phenylalanine by *Tc*PAM.

of (3S)-α-tyrosine to (3S)-β-tyrosine, while *Tc*PAM catalyze the isomerization of (2S)-α- phenylalanine to (2R)-β- phenylalanine [17].

From the view point of cofactor dependency and amino acid sequence similarity, PAM and TAM belong to the same family, which also includes several ammonia lyases. Because these enzymes contain the 5-methylene-3,5-dihydroimidazol-4-one (MIO) motif in their active sites, they are usually called MIO-dependent enzymes. In fact, MIO can be formed autocatalytically from the internal tripeptide Ala-Ser-Gly [27–29].

Since the initial discovery of MIO in the X-ray crystal of histidine ammonia lyase (HAL), the mechanistic role of MIO, and the mechanism of MIO-dependent lyase have been discussed in literature for many years [20,30–32]. In general, two different mechanisms have been proposed for the lyase reaction in which MIO either reacts with the amine or with the aromatic ring of the substrate to generate two covalent adducts. Both pathways lead to the deprotonation and elimination of ammonia to form the conjugated olefin. On the basis of structural homology and experimental findings, the mechanism of aminomutases is suggested to be an extension of the lyase chemistry with the re-addition of the amine via conjugate addition. Thus, two mechanisms have been proposed for aminoumutases (Scheme 2). One is an amino-MIO adduct mechanism (Scheme 2A), and the other is a Friedel–Crafts-type (FC) reaction mechanism (Scheme 2B). In the first mechanism, the amino group of the substrate acts as a nucleophile and attacks the methylidene of MIO through a conjugate addition. Ammonia is then expelled from the N-alkylated substrate through an α,β-elimination, and the α,β-unsaturated carboxylic acid is formed. Finally, the amino group is rebound to the α,β-unsaturated carboxylic acid, and the corresponding β-amino acid is formed. In the second proposed mechanism, the reaction is initiated by electrophilic attack of the aromatic ring on MIO, which acts as a Lewis acid. This Friedel–Crafts-type mechanism leads to removal of the β-proton through a carbocation intermediate, which is followed by the elimination of ammonia and regeneration of the MIO group.

From Scheme 2, one can see that both pathways undergo an abstraction of β-hydrogen of the substrate and formation of a cinnamic acid intermediate. The key difference between the two mechanisms is that in the amino-MIO adduct mechanism, the nucleophile is the MIO-bound amine, whereas free ammonia serves this function in Friedel–Crafts type mechanism. To further probe the mechanism of MIO-dependent enzymes, a number of studies have been carried out. The co-crystal structures of *Sg*TAM with an inhibitor (α,α-difluoro-β-tyrosine) by Bruner et al. provided strong evidence that the MIO-based enzymes use covalent catalysis (amino-MIO adduct mechanism) [33]. Recent ONIOM quantum mechanics/molecular mechanics calculations on tyrosine ammonia lyase (TAL) also suggested that the TAL catalyzed reaction prefers the amino-MIO adduct mechanism [34]. The hypothetical Friedel–Crafts mechanism was ruled out due to the high relative energy of FC intermediate; the ammonia elimination proceeds via an amino-MIO intermediate through the concerted (E2) route. Bornscheuer et al. studied the possibility of the two mechanisms of phenylalanine and tyrosine ammonia lyases (PAL/TAL) using automated docking and molecular dynamics simulations [35] and deduced that the Glu484 residue in PAL/PAM prevents the MIO group from an attack on the amino group of the substrate, implying the Friedel–Crafts type mechanism occurs. It should however be noted that the protonated states of the substrate and the key residues were not considered which would lead to different reaction pathways. Additionally, the details of catalytic reaction and stereochemistry were not addressed.

Up to now, the controversy surrounding the mechanism is ongoing, and the nature of stereochemical control is not well understood. We hypothesize that the reaction mechanism of these enzymes may depend on the different structures of their active sites. In some cases, the reaction may follow amino-MIO adduct mechanism, whereas in other situations, the reaction may follow a Friedel–Crafts type mechanism. As for the stereochemistry, similar mechanisms may also lead to different products. For example, *Tc*PAM catalyze the production of β-phenylalanine, which is the enantiomer of the product catalyzed by *Pa*PAM, and also different to the (3S)-stereochemistry found in the product of the *Sg*TAM reaction. It has been proposed recently that in *Tc*PAM-catalyzed reaction, the cinnamate intermediate undergoes an intramolecular rotation about the C1-Cα/C4-Cβ [21]. The amino group of amino-MIO reattaches on the opposite face from which they originated. The stereochemistry of *Tc*PAM is uncommon compared to the aminomutase mechanisms examined so far.

It is noted that neither of these two mechanisms is without critics, and there is not yet a consensus on the *Tc*PAM catalyzed enzymatic mechanism. As far as we know, there are few established theoretical works directed to the understanding of the detailed reaction mechanism. For this reason, the principal aim of this paper is to gain insights into the mechanism of the whole *Tc*PAM catalyzed reaction. The quantum chemical methods used in this work have been successfully applied in recent years to study the enzymatic reaction mechanism; an appropriate model of the enzyme active site is used, with the rest of enzyme usually being considered homogenously polarizable and can therefore normally be treated by dielectric cavity techniques [36–40]. Although these computational models are relatively small, they are still reasonably adequate in describing the enzymatic reaction occurs in the active site, and in particularly, in distinguishing alternative mechanisms. It is noted that combined quantum mechanics and molecular mechanics (QM/MM) methods have been increasingly developed in recent years to investigate the fundamental and practical problems in enzymology [41–43]. Compared to cluster models, the influences of enzyme environment are well considered in the QM/MM model, but it is usually more expensive than a simple QM calculation. To increase the computation efficiency, in the present paper, density functional theory (DFT) calculations with the QM method on a cluster model were performed with the aim to resolve the controversial question of an alternative mechanism, and qualitatively understand the transition state structures and energetics of the two reaction mechanisms. Emphasis is given on the distinction between the different mechanisms, and a preferred mechanism will be obtained according our calculations. The important residues mutated in the experiments will be calculated in our on-going QM/MM studies to explain that how the mutagenesis influence the catalytic rate.

2. Computational details

2.1. Computational methods

Theoretical calculations presented herein were performed using the density functional theory (DFT) functional B3LYP [44–48] as implemented in the Gaussian03 program package [49]. The geometries of reactants, products, intermediates, and transition states

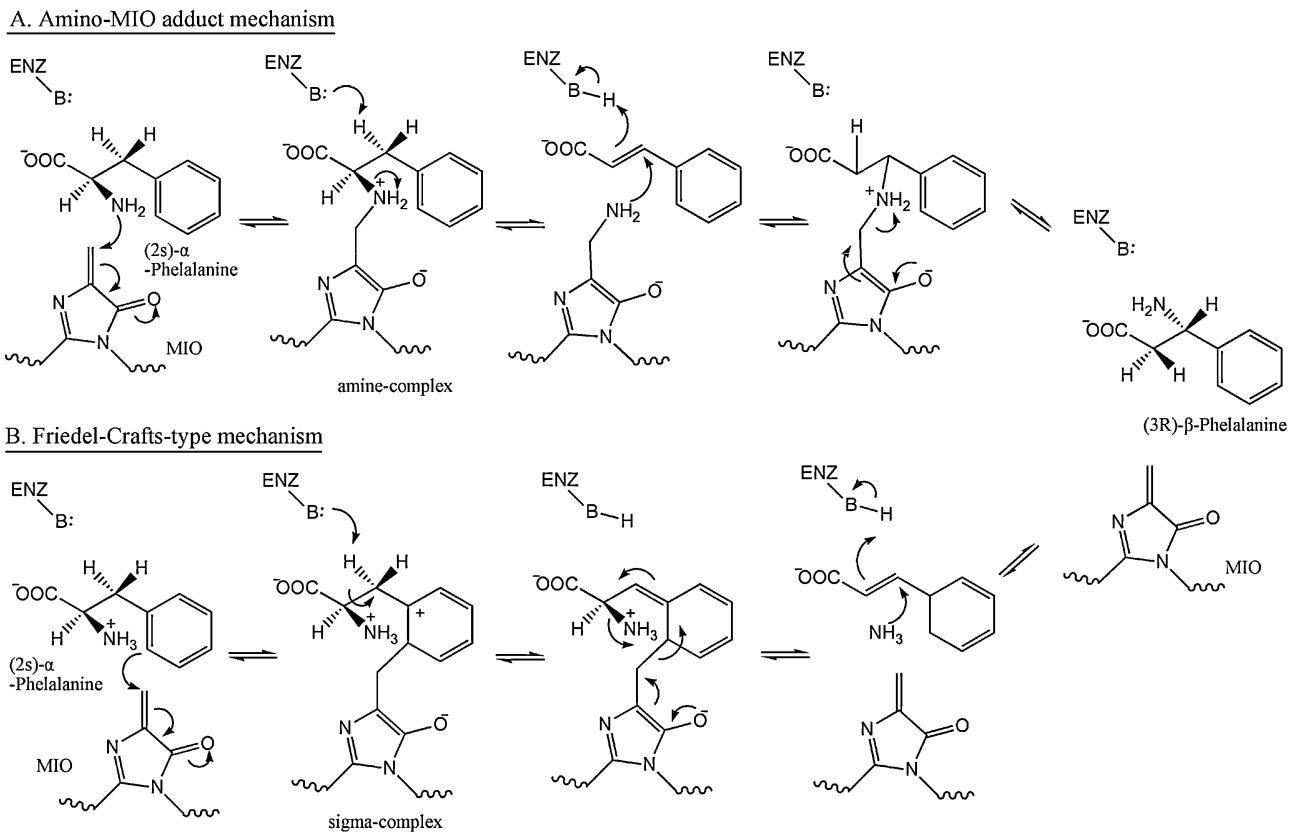

Scheme 2. Two proposed mechanisms for the conversion of substrate to product for MIO-dependent lyase and mutase enzymes: (A) the amino-MIO adduct mechanism and (B) Friedel–Crafts-type reaction mechanism.

involved in the reaction have been optimized using the 6-31G(d,p) basis set in the gas phase. In the model, the truncation atoms were fixed to their crystallographically observed positions. Single point energy calculations were performed at the B3LYP/6-311++G(2d,2p) level of theory by using the polarizable continuum model (PCM), in which the solvation effect of water had been considered by using a relatively simple self consistent reaction field (SCRF) model using the UAHF set of solvation radii to build the cavity for the solute in the gas-phase [50,51]. A dielectric constant of $\varepsilon = 4$ was chosen to describe the protein environment of the active site in agreement with previous suggestions [36–40]. All of the reaction pathways were subjected to the intrinsic reaction coordinate (IRC) analyses, in order to trace their paths and confirm that the optimized TS structures connect the corresponding two structures residing at minima. Frequency calculations were performed in the gas phase for each optimized structure with the 6-31G(d,p) basis set to obtain the zero-point vibrational energies, and to confirm that all of the optimized geometries correspond to a local minimum that has no imaginary frequency mode or a saddle point that has only one imaginary frequency mode. Since some atoms were frozen to their crystallographic positions, a few small negative eigenvalues usually appear, typically in the order of 10 cm^{-1}. These frequencies do not contribute significantly to the zero-point energies and can be ignored. The final reported energies are obtained from PCM single-point energy calculations at the B3LYP/6-311++G(2d,2p) level of theory based on the optimized structures at the B3LYP/6-31G(d,p) level in the gas, plus gas-phase zero-point corrections.

2.2. Active site model

A large computational model was built up on the basis of a recent X-ray crystal structure of *Tc*PAM complexed with cinnamic acid (PDB code: 3NZ4) [21]. The active site taken from the crystal structure is shown in Fig. S1. The cinnamic acid is bound in the active site, lying about 3.4 Å above the methylidene carbon of MIO. To obtain the reactant of the reaction, the cinnamic acid was removed, and the natural substrate (2S)-α-phenylalanine, optimized at the B3LYP/6-31G(d,p) level with the Gaussian 03 package [49], was placed into the active site using the Autodock program [52]. Leu104 and Phe371 only provide hydrophobic interaction to the substrate and were not kept in the computational model. Important residues (Tyr80, Phe86, Gly87, Tyr322, Arg325, Glu455 and Asn458) which directly form an extensive network of hydrogen bonds between the substrate and MIO were all included. The obtained model consists of 118 atoms with a total charge of -2. Asn458 was modeled by an acetamide molecule, and Glu455 by an acetate molecule. Tyr80 and Tyr322 are both modeled by a methylphenol molecule, Arg325 included a guanidine group was truncated to the δ-carbon. N-methylacetamide was used to simulate Phe86 and Gly87. Arg325 and Tyr322 were set in their protonated states, and all of the other residues in their neutral states. To avoid artificial movements of various groups, some atoms were forced into their crystallographic positions during the optimization and such indicated by the asterisk in the figures.

3. Results and discussion

3.1. The amino-MIO adduct mechanism

The elementary steps involved in the catalytic reaction were determined through our calculations, as shown in Scheme 3. The entire process is divided into three main steps: ammonia elimination, C1—Cα bond rotation, and (3R)-β-phenylalanine formation. The optimized structure of the reactant complex (Re) is shown in

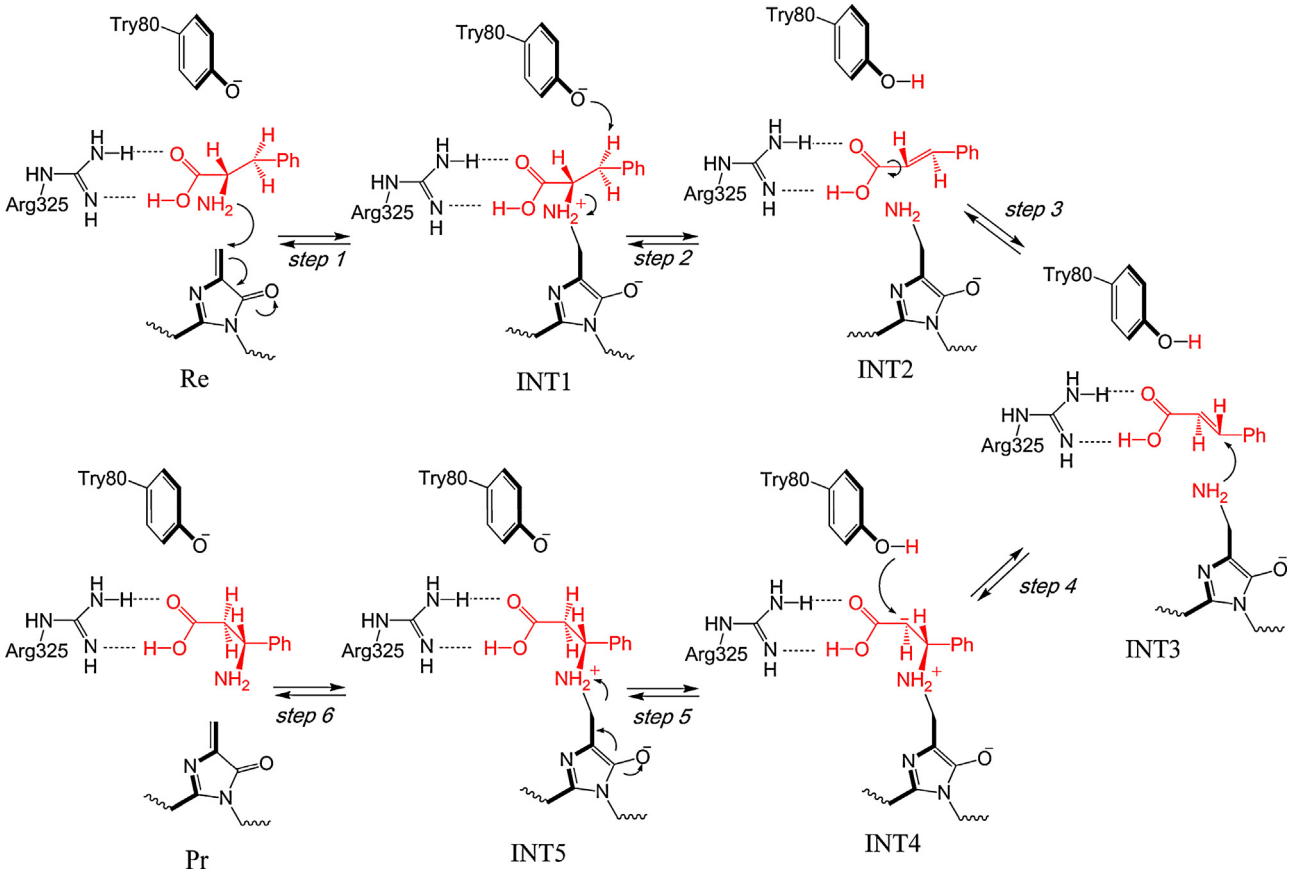

Scheme 3. Proposed catalytic process of the amino-MIO adduct mechanism for *Tc*PAM.

Fig. 1A, and the transition states, intermediates and product complex (Pr) are shown in Fig. 2.

3.1.1. Ammonia elimination

In our calculations, reactant complex Re (Fig. 1A) was taken as the initial structure of this reaction. The Arg325 residue was set at its protonated state, and the substrate was in the anionic form. During the optimization, a proton was immediately transferred from one amino group of Arg325 to the carboxylic anion of substrate. As a result, both of the substrate and Arg325 are in the neutral form in this model. The substrate is anchored by an extensive network of hydrogen bonds from the active site residues; Asn458 and Arg325 forms a hydrogen bond and a salt bridge, respectively, with the carboxyl group of the substrate, while. Tyr322 forms two hydrogen bonds with the amino group of the substrate and MIO. The distance between the MIO methylene carbon and the amino group of

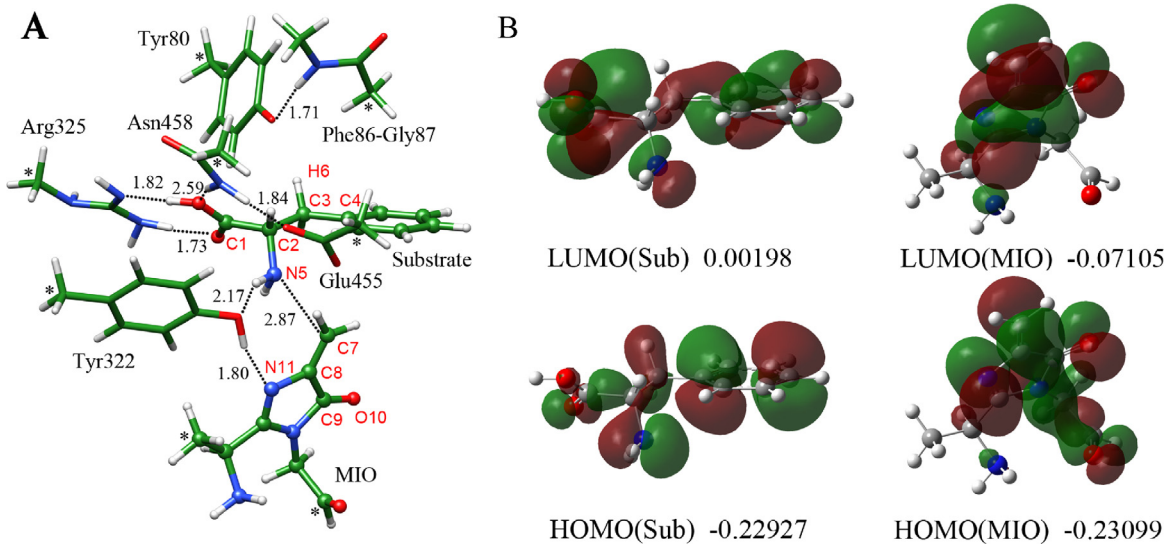

Fig. 1. (A) Optimized structure (Re) of the *Tc*PAM active site with the substrate molecule, (2*S*)-β-phenylalanine, for the amino-MIO adduct mechanism. Atoms marked with small arrows were kept frozen during the geometry optimizations. Distances are in angstroms. (B) B3LYP frontier molecular orbitals and orbital energies (in atom units) of the substrate (Sub) and MIO.

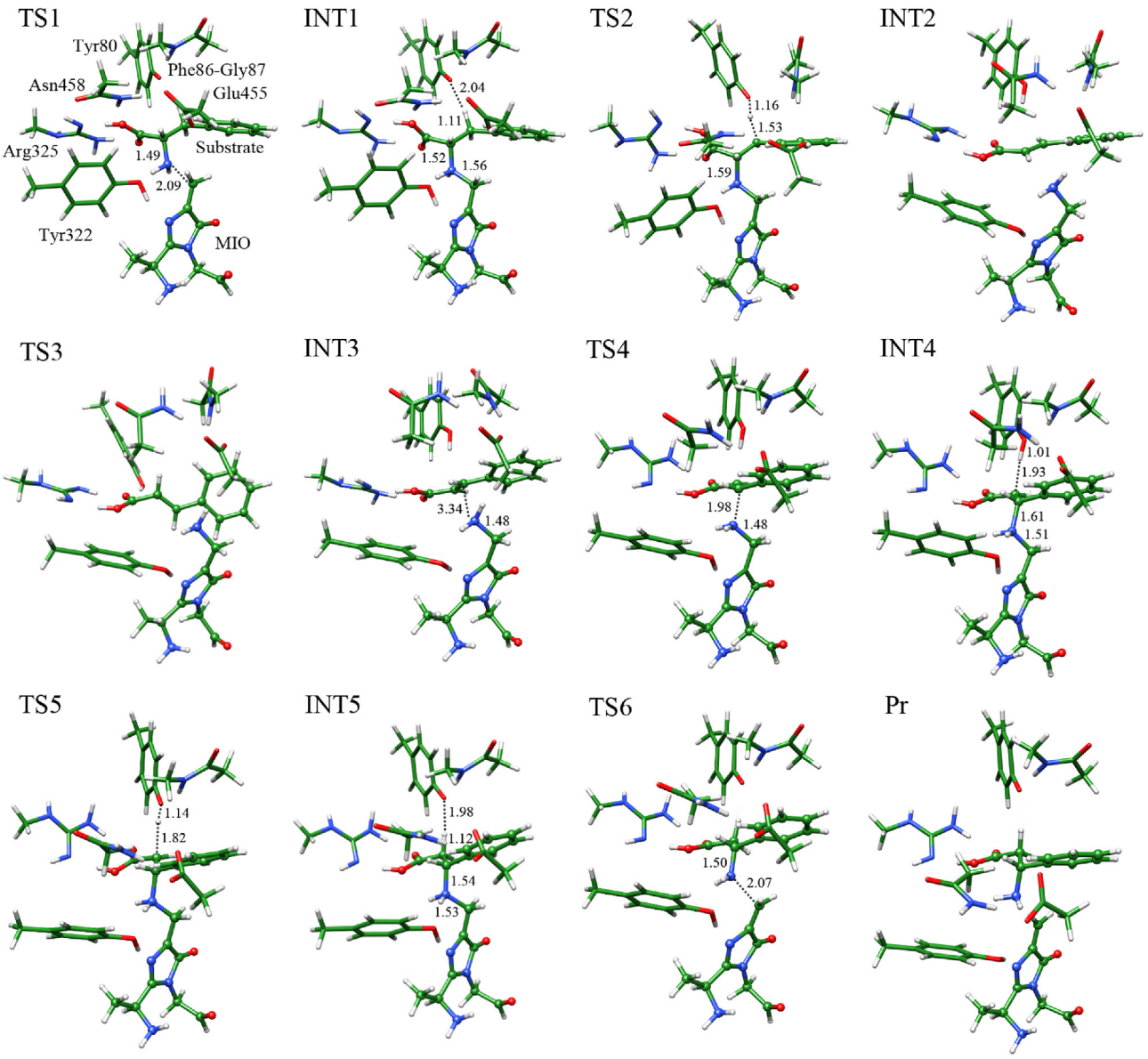

Fig. 2. Optimized structures of the transition states, intermediates and product complex (Pr) for the amino-MIO adduct mechanism.

the substrate is 2.87 Å. Subsequently, molecular orbital calculations were further performed to analyze the reactivity of the substrate and MIO. It has been reported that the shape and symmetry properties of KS orbitals are very similar to those calculated by HF methods [53,54], therefore, the KS orbitals are used for the following analysis. The most important frontier molecular orbitals such as the highest occupied molecular orbital (HOMO) and lowest unoccupied molecular orbital (LUMO) are responsible for the reaction between methylene and the amino group of the substrate. The HOMO and LUMO orbitals and orbital energies of the substrate (described as Sub) and MIO are depicted in Fig. 1B. For the substrate molecule, the HOMO orbital lies at −0.22928 a.u. and the LUMO orbital lies at 0.00198 a.u. For MIO, the HOMO orbital is at −0.23099 a.u. and the LUMO orbital is at −0.07105 a.u. Among these orbitals, the HOMO of substrate and LUMO of MIO are very close in energy and matching orbital symmetries. Therefore, according to the frontier orbital theory, the substrate HOMO interacts with the LUMO of MIO producing the greatest stabilization, and the reaction between the amino group of the substrate and the methylene carbon of MIO may easily occur.

As shown in Fig. 2, the nucleophilic attack of the amino group of substrate on the methylene carbon of MIO undergoes a transition state (TS1) with an energy barrier of 7.8 kcal/mol. The corresponding energy profile in the reaction path are shown in Fig. 3. In TS1,

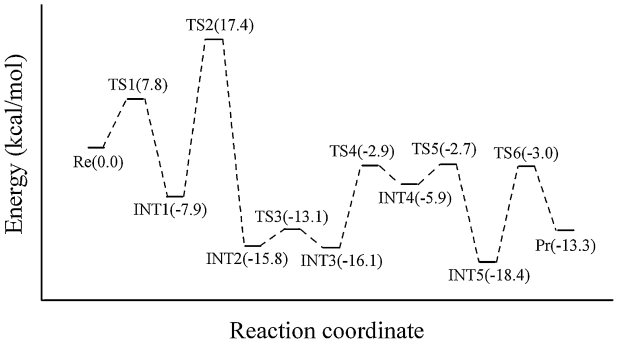

Fig. 3. Energy profile for the catalytic reaction.

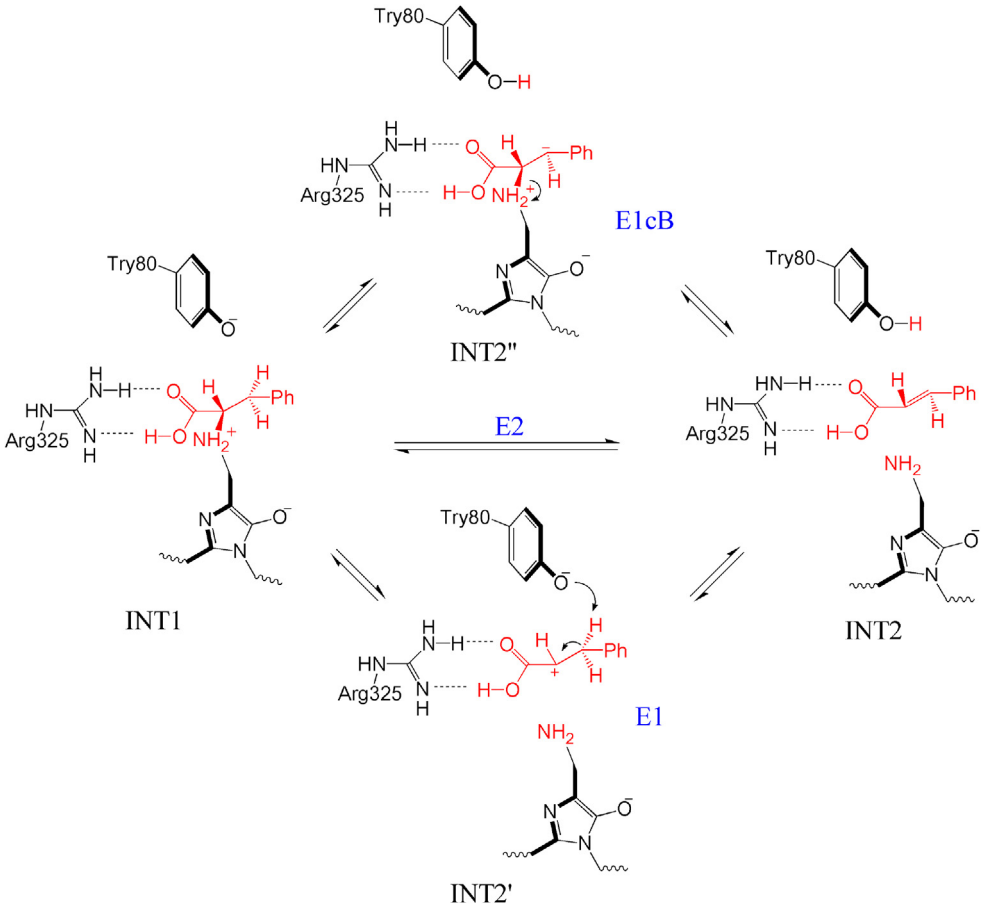

Scheme 4. Three alternative pathways (E_1, E_1cB, E_2) proposed for the ammonia elimination from the amino-MIO intermediate.

the distance of N5 and C7 (the atomic labels are shown in Fig. 1A) decreases to 2.09 Å, and carbon C7 changes its hybridization from sp^2 to sp^3, while remaining negatively charged (−0.18 *e*). After TS1, the amino-MIO adduct INT1 is formed in which the distance of C7—N5 and C2—N5 are 1.56 and 1.52 Å, respectively.

The three alternative pathways (E1, E1cB, E2, shown in Scheme 4) for the ammonia elimination from the amino-MIO intermediate (INT1) are then considered. The E1- and E1cB-like elimination pathways are both ruled out based on our calculations because all of the structures constructed for the E1 intermediate (carbocationic) and E1cB intermediate (carbanionic) result in INT1 or INT2. Furthermore, we have obtained the transition state (TS2) for the concerted process which is characterized by an imaginary frequency of 831i cm^{-1}. While the proton H6 of the β-carbon C3 transfers to Tyr80, the C2-N5 bond is sensibly elongated with a distance of 1.59 Å simultaneously. The energy barrier for this step is 25.3 kcal/mol. It is concluded that the ammonia elimination reaction follows the E2 mechanism where the hybridization of both C2 and C3 change from sp^3 to sp^2, and the α,β-unsaturated carboxylic acid cinnamic acid is formed in INT2. The E2 mechanism for the elimination reaction obtained from our calculations is consistent with the results of the recent TAL theoretical studies by László Poppe [34]. The N-MIO intermediate that converses to (E)-counmarate catalyzed by TAL also undergoes a simultaneous E2 amino elimination.

3.1.2. C1—Cα bond rotation

In order to obtain the transoid acrylate product, the amino group of amino-MIO must reattach to the Cβ on the opposite side of the cinnamic acid. A possible explanation is that the cinnamate intermediate first undergoes a rotation of C1—Cα bond, as described in Fig. 4, where the transition state, TS3, is characterized by an imaginary frequency of 176i cm^{-1}. In INT2, the NH_2 group is far away from Cβ with a distance of 4.2 Å, but in INT3 the NH_2 group is close to Cβ with a distance of 3.3 Å and faces to the opposite side of cinnamate. The dihedral angles of O—C1—C2—C3 are 1.79° in INT2, −90.95° in TS3, and 177.95° in INT3, thus indicating a complete rotation of C1—Cα by approximately 180°. The calculated energy barrier for this step is 2.7 kcal/mol. INT3 lies only 0.3 kcal/mol lower than INT2, showing that the rotamers of INT2 and INT3 are energetically equivalent, which is also suggested by the K_{ep} ~1 for the *Tc*PAM reaction [55]. During the rotation, the salt bridge is consistently formed between the carboxylate group of cinnamate and the guanidine group of Arg325; Tyr80 is situated above the Cα—Cβ bond with a distance of ~2.8 Å and there is no steric clash during the rotation.

This rotation is unusual among all aminomutase mechanisms examined so far. The *Sg*TAM reaction was found to isomerize (S)-α-tyrosine to (S)-β-tyrosine in which the amino group migrated from Cα to Cβ across the same face of the coumarate intermediate. By comparing the active sites of *Tc*PAM[21] and *Sg*TAM [33], it was observed that there are subtle structural differences that may cause stereodifferentiation. In the *Tc*PAM structure, there is a direct hydrophobic interaction between Leu104 with the aromatic ring of the phenylalanine substrate, while in the *Sg*TAM, His93 and Tyr415 form two hydrogen bonds to the hydroxyl group of the tyrosine substrate. These two hydrogen bonds lead to the rotation of the aromatic ring of the substrate by about 40 °compared with that of the ring of the cinnamate substrate in *Tc*PAM, which positions the amino group within close proximity to reattach to the Cβ of the

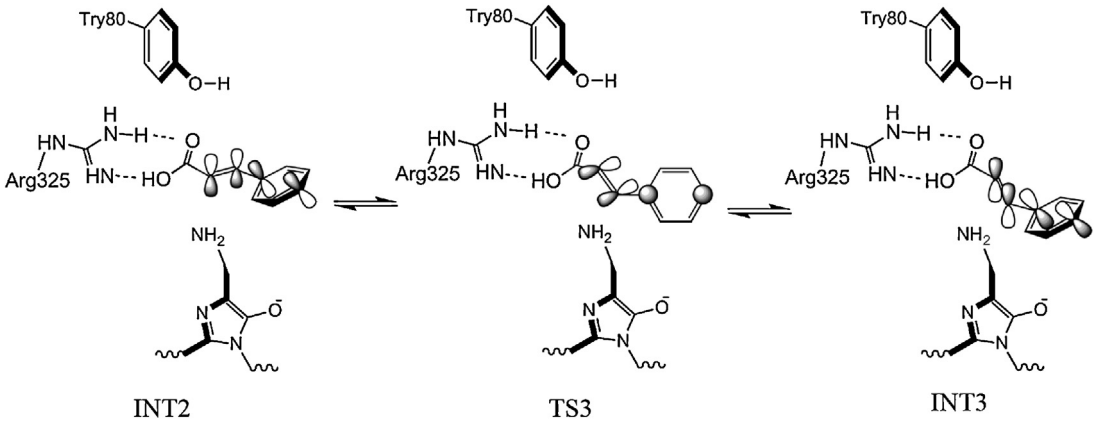

Fig. 4. Proposed course for the C1—Cα bond rotation. The p-oribtals on the C=C and the ring are only provided for perspective.

acrylate intermediate. As to *Tc*PAM, only after the cinnamate intermediate undergoes a C1—Cα rotation is the amino group able to rebind to Cβ. The calculated mechanism is consistent with that proposed by Wu, B. in that only one bond rotatation is required since the rotations of both the C1—Cα and the C4—Cβ bonds is energetically burdensome [56]. The central question regarding how *Tc*PAM catalyze an opposite stereoisomer of its β-amino acid product compared to that of *Sg*TAM enzyme is successfully answered.

3.1.3. (3R)-β-phenylalanine formation

The amino-MIO rebounds to the opposite face of cinnamate in step 4. From INT3 to TS4, C3—N5 decreases from 3.34 to 1.98 Å, and meanwhile the hybridization of C3 changes from sp^2 to sp^3. This step occurs with a barrier of 13.2;kcal/mol and endothermic relative to INT3 by 10.2 kcal/mol. In INT4, the distances between the C3—N5 and N5—C7 bonds are 1.61 Å and 1.51 Å, respectively. The proton H6 transfers back easily from Tyr80 to C2 of β-complex with a low barrier of 3.2 kcal/mol. In the final step (step 6), the N5—C7 bond breaks and leads to the reaction product with an energy barrier of 15.4 kcal/mol.

3.2. The Friedel–Crafts-type mechanism

In our exploration of possible reaction mechanisms, the Friedel–Crafts-type mechanism has also been studied. As shown in Scheme 2B, MIO is proposed undergo nucleophilic attack by the aromatic ring, and one ammonia molecule is eliminated. Accordingly, the substrate is set to its zwiterionic state (described as Sub') in the constructed model. The optimized structure and B3LYP frontier molecular orbitals and orbital energies of the Sub' and MIO are shown in Fig. 5. There is a small change in the structure of the active site compared with the reactant structure in the amino-MIO adduct mechanism (Fig. 1A); the carboxyl group of Sub' is still anchored by Arg325, but the C1—C2 bond has rotated 96° relative to the original C1—C2 bond of the Sub. As well, the protonated amino group forms two hydrogen bonds to Glu455 and Phe86. The dihedral angle of the benzene ring and the carboxyl group is 109.9° in Sub', while this value is 30.6° in Sub. In order to obtain the σ-complex carbocation intermediate described in Scheme 2B, we have performed a series of constrained optimizations by fixing the C5—C7 distance. The calculated energy profile, along with the variation of the C5—C7 distance, was plotted in Fig. S2. Unfortunately, the energies are increased steadily, and no transition state was found. The last structure was then optimized, but resulted in what was the structure of the reactant due to large steric distortions. Interestingly, when the proton atom was abstracted by Tyr80, an intermediate, which lies 39.5 kcal/mol higher than the reactant, was obtained (shown in Fig. S3). This energy can be considered relatively high, and this pathway can be excluded. Furthermore, as shown in Fig. 5B, the HOMO and LUMO orbital energies of the substrate are −0.19641 and −0.02477 a.u., respectively, and those of MIO are −0.23099 and −0.07105 a.u. respectively. It can be seen that the energy of HOMO of Sub' is closer to the LUMO of MIO than the HOMO of Sub. However, the FC-mechanism can be ruled out because the HOMO of Sub' involves the carboxylate group, and not the benzene ring. All these analyses show that the Friedel–Crafts-type mechanism can be excluded.

3.3. Discussion

According to these calculation data, the Friedel–Crafts-type mechanism may be excluded, and the amino-MIO adduct mechanism is more favorable both from thermodynamic and kinetic points of view. The overall reaction is exothermic with 13.3 kcal/mol, and the rate-limiting step is the concerted reaction of the deprotonation at the β-position and ammonia elimination through an E2 mechanism with an energy barrier of 25.3 kcal/mol. The dynamics of the Cβ—H bond of the substrate measured by experiments also indicated that the C—H bond cleavage was likely rate limiting [55]. The free energy of this step is calculated to be 13.1 kcal/mol. Furthermore, the semi-classical kinetic isotope effect (KIE) [57–60] was calculated to approximately evaluate the nuclear quantum dynamical effect on the rate-limiting step. The required free energy of activation and vibrational frequencies were determined at the B3LYP/6-31G(d,p) level using the Gaussian03 package [49], as shown in Table S1. The semi-classical KIE value is 4.6 and the Wigner-corrected KIE value is 5.5, implying that the quantum mechanical tunneling effect is not significant in this step.

The mechanism for MIO-dependent enzymes has been controversially discussed for many years. In our calculations, the geometrical structures and the frontier molecular orbital analysis show that MIO preferentially reacts with amino group of phenylalanine, but not with the aromatic ring. We therefore suggest that the MIO-dependent enzymes using phenylalanine as the substrate will share the similar catalytic pathway, such as PAL, PAM. The elementary steps obtained from the calculations account for the observed kinetic isotope observed in experiments. The intermediate cinnamic acid also agrees well with the crystal structure (PDB code: 3NZ4) [21,55]. Moreover, calculations have elucidated the role of the catalytically relevant residues in the active site; Tyr80 is identified as critical in the *Tc*PAM reaction by shuttling the proton between the α- and β-positions and Tyr322 forms a hydrogen bond to the nitrogen atom of MIO to assist the electrophilic character of MIO. Arg325 strongly anchors the carboxylate of the substrate

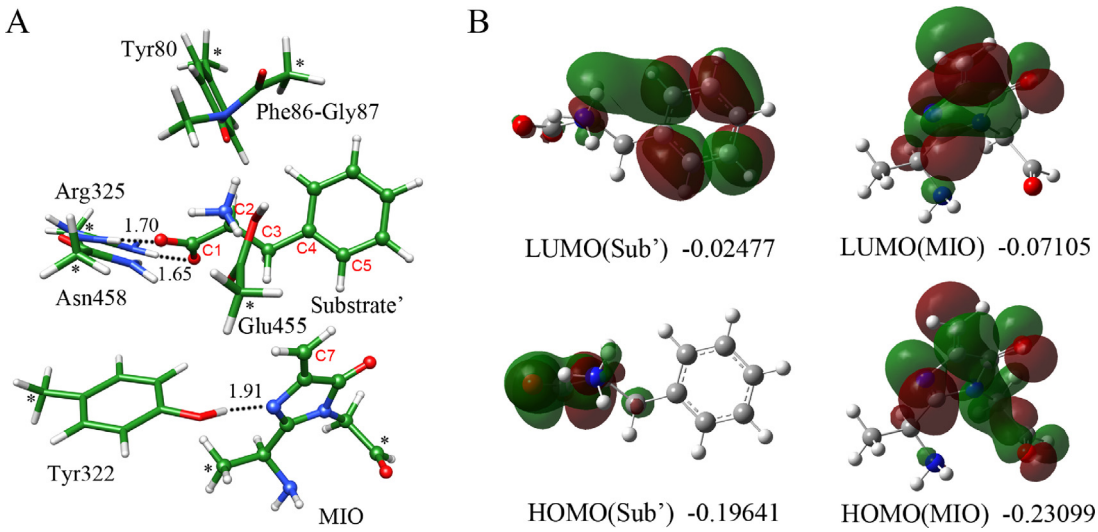

Fig. 5. (A) Optimized structure of the *Tc*PAM active site with the substrate' for the Friedel–Crafts-type mechanism. (B) B3LYP frontier molecular orbitals and orbital energies (in atom units) of the substrate' (Sub') and MIO.

through a salt bridge interaction, which serves to fix one side of the substrate throughout the catalytic reaction. The other residues Phe86, Gly87, Glu455, and Asn458 contribute to maintaining the network of hydrogen bonds in the active site.

4. Conclusion

In this work, we have presented a theoretical investigation of the catalytic mechanism of *Tc*PAM by employing the B3LYP density functional theory. The main results can be summarized as follows:

(1) The reaction proceeds through an amino-MIO adduct mechanism, but not a Friedel–Crafts-type mechanism. The Friedel–Crafts mechanism may be ruled out mainly because of its high energy and also by the frontier molecular orbitals analysis. In the amino-MIO adduct mechanism, the deprotonation at the β-position and ammonia elimination occurs on the amino-MIO adduct through an E2 mechanism.
(2) The stereochemistry of the *Tc*PAM reaction can be achieved by rotation of the cinnamate intermediate around the C1—Cα bond prior to rebinding of the amino group at the β-position of the intermediate. This would be the reason that *Tc*PAM catalyze the opposite stereochemistry production compared with *Pa*PAM and *Sg*TAM.
(3) The role of several important active-site residues are illustrated according to our calculations. The substrate is anchored in the active site by an extensive network of hydrogen bonds between its amino group and Tyr322, as well as between its carboxylate group, Arg325, and Asn458. We have confirmed the role of Tyr80 in shuttling the proton between the α- and β-positions as the enzymatic base.
(4) The mechanism described here for *Tc*PAM is consistent with several experimental results, and provides strong theoretical support for the stereochemistry. This is expected to shed light on the preparation of the chiral building blocks.

Acknowledgment

This work was supported by the National Natural Science Foundation of China (21173129, 21373125).

Appendix A. Supplementary data

Supplementary data (including data for KIE calculations, the active site taken from the X-ray crystal structure of *Tc*PAM, approximate potential energy profile of the formation of carbocation intermediate, and the optimized intermediate structure for the FC mechanism) associated with this article can be found, in the online version, at http://dx.doi.org/10.1016/j.jmgm.2013.09.010.

References

[1] J.M. Poston, Leucine 2,3-aminomutase, an enzyme of leucine catabolism, J. Biol. Chem. 251 (1976) 1859–1863.
[2] T.P. Chirpich, V. Zappia, R.N. Costilow, H.A. Barker, Lysine 2,3-aminomutase. Purification and properties of a pyridoxal phosphate and S-adenosylmethionine-activated enzyme, J. Biol. Chem. 245 (1970) 1778–1789.
[3] P.C. Prabhakaran, N.-T. Woo, P.S. Yorgey, S.J. Gould, Biosynthesis of blasticidin s from L-a-arginine. Stereochemistry in the arginine-2, 3-aminomutase reaction, J. Am. Chem. Soc. 110 (1988) 5785–5791.
[4] D.L. Steer, R.A. Lew, P. Perlmutter, A.I. Smith, M.I. Aguilar, Beta-amino acids: versatile peptidomimetics, Curr. Med. Chem. 9 (2002) 811–822.
[5] G. Lelais, D. Seebach, Beta2-amino acids-syntheses, occurrence in natural products, and components of beta-peptides1,2, Biopolymers 76 (2004) 206–243.
[6] D. Seebach, M. Overhand, F.N.M. Kuhnle, B. Martinoni, L. Oberer, U. Hommel, H. Widmer, β-Peptides: synthesis by Arndt-Eistert homologation with concomitant peptide coupling. Structure determination by NMR and CD spectroscopy and by X-ray crystallography. Helical secondary structure of a β-hexapeptide in solution and its stability towards pepsin, Helv. Chim. Acta 79 (1996) 913–941.
[7] M. Liu, M.P. Sibi, Temperature dependent reversal of stereochemistry in enantioselective conjugate amine additions, Tetrahedron 58 (2002) 7991–8035.
[8] D. Pena, A.J. Minnaard, J.G. de Vries, B.L. Feringa, Highly enantioselective rhodium-catalyzed hydrogenation of beta-dehydroamino acid derivatives using monodentate phosphoramidites, J. Am. Chem. Soc. 124 (2002) 14552–14553.
[9] A. Duursma, A.J. Minnaard, B.L. Feringa, Highly enantioselective conjugate addition of dialkylzinc reagents to acyclic nitroalkenes: a catalytic route to 2-amino acids, aldehydes, and alcohols, J. Am. Chem. Soc. 125 (2003) 3700–3701.
[10] F. Gessier, L. Schaeffer, T. Kimmerlin, O. Flogel, D. Seebach, Preparation of β2-amino acid derivatives (β^2hThr, β^2hTrp, β^2hMet, β^2hPro, β^2hLys, pyrrolidine-3-carboxylic acid) by using DIOZ as chiral auxiliary, Helv. Chim. Acta 88 (2005) 2235–2249.
[11] W. Liu, S.D. Christenson, S. Standage, B. Shen, Biosynthesis of the enediyne antitumor antibiotic C-1027, Science 297 (2002) 1170–1173.
[12] X. Yin, T. O'Hare, S.J. Gould, T.M. Zabriskie, Identification and cloning of genes encoding viomycin biosynthesis from *Streptomyces vinaceus* and evidence for involvement of a rare oxygenase, Gene 312 (2003) 215–224.
[13] K. Walker, R. Croteau, Taxol biosynthetic genes, Phytochemistry 58 (2001) 1–7.
[14] D.J. Aberhart, J.A. Cotting, Mechanistic studies on lysine 2,3-aminomutase: carbon-13-deuterium crossover experiments, J. Chem. Soc. Perkin Trans. 1 (1988) 2119–2122.
[15] D.J. Aberhart, S.J. Gould, H.J. Lin, T.K. Thiruvengadam, B.H. Weiller, Stereochemistry of lysine 2,3-aminomutase isolated from *Clostridium subterminale* strain SB4, J. Am. Chem. Soc. 105 (1983) 5461–5470.

[16] R.J. Parry, Z. Kurylo-Borowska, Biosynthesis of amino acids. Investigation of the mechanism of beta-tyrosine formation, J. Am. Chem. Soc. 102 (1980) 836–837.
[17] S.D. Christenson, W. Liu, M.D. Toney, B. Shen, A novel 4-methylideneimidazole-5-one-containing tyrosine aminomutase in enediyne antitumor antibiotic C-1027 biosynthesis, J. Am. Chem. Soc. 125 (2003) 6062–6063.
[18] J. Rétey, F. Kunz, D. Arigoni, T.C. Stadtman, Zur kenntnis der beta-lysin-mutase-reaktion: mechanismus und sterischer verlauf, Helv. Chim. Acta 61 (1978) 2989–2998.
[19] H.P. Chen, S.H. Wu, Y.L. Lin, C.M. Chen, S.S. Tsay, Cloning, sequencing, heterologous expression, purification, and characterization of adenosylcobalamin-dependent D-ornithine aminomutase from *Clostridium sticklandii*, J. Biol. Chem. 276 (2001) 44744–44750.
[20] N.A. Magarvey, P.D. Fortin, P.M. Thomas, N.L. Kelleher, C.T. Walsh, Gatekeeping versus promiscuity in the early stages of the andrimid biosynthetic assembly line, ACS Chem. Biol. 3 (2008) 542–554.
[21] L. Feng, U. Wanninayake, S. Strom, J. Geiger, K.D. Walker, Mechanistic, mutational, and structural evaluation of a taxus phenylalanine aminomutase, Biochemistry 50 (2011) 2919–2930.
[22] N.D. Ratnayake, U. Wanninayake, J.H. Geiger, K.D. Walker, Stereochemistry and mechanism of a microbial phenylalanine aminomutase, J. Am. Chem. Soc. 133 (2011) 8531–8533.
[23] D. Röther, L. Poppe, S. Viergutz, B. Langer, J. Rétey, Characterization of the active site of histidine ammonia-lyase from *Pseudomonas putida*, Eur. J. Biochem. 268 (2001) 6011–6019.
[24] Y. Asano, Y. Kato, C. Levy, P. Baker, D. Rice, Structure and function of amino acid ammonia-lyases, Biocatal. Biotransform. 22 (2004) 133–140.
[25] M. Rettig, A. Sigrist, J. Rétey, Mimicking the reaction of phenylalanine ammonia lyase by a synthetic model, Helv. Chim. Acta 83 (2000) 2246–2265.
[26] W. Szymanski, B. Wu, B. Weiner, S. de Wildeman, B.L. Feringa, D.B. Janssen, Phenylalanine aminomutase-catalyzed addition of ammonia to substituted cinnamic acids: a route to enantiopure alpha- and beta-amino acids, J. Org. Chem. 74 (2009) 9152–9157.
[27] T.F. Schwede, J. Retey, G.E. Schulz, Crystal structure of histidine ammonia-lyase revealing a novel polypeptide modification as the catalytic electrophile, Biochemistry 38 (1999) 5355–5361.
[28] K.D. Walker, K. Klettke, T. Akiyama, R.J. Croteau, Cloning, Heterologous expression, and characterization of a phenylalanine aminomutase involved in taxol biosynthesis, Biol. Chem. 279 (2004) 53947–53954.
[29] J.C. Calabrese, D.B. Jordan, A. Boodhoo, S. Sariaslani, T. Vannelli, Crystal structure of phenylalanine ammonia lyase: multiple helix dipoles implicated in catalysis, Biochemistry 43 (2004) 11403–11416.
[30] S. Rachid, D. Krug, K.J. Weissman, R. Muller, Biosynthesis of (R)-beta-tyrosine and its incorporation into the highly cytotoxic chondramides produced by *Chondromyces crocatus*, J. Biol. Chem. 282 (2007) 21810–21817.
[31] D. Krug, R. Muller, Discovery of additional members of the tyrosine aminomutase enzyme family and the mutational analysis of CmdF, ChemBioChem. 10 (2009) 741–750.
[32] S.G. Van Lanen, T.J. Oh, W. Liu, E. Wendt-Pienkowski, B. Shen, Characterization of the maduropeptin biosynthetic gene cluster from *Actinomadura madurae* ATCC 39144 supporting a unifying paradigm for enediyne biosynthesis, J. Am. Chem. Soc. 129 (2007) 13082–13094.
[33] C.V. Christianson, T.J. Montavon, G.M. Festin, H.A. Cooke, B. Shen, S.D. Bruner, The mechanism of MIO-based aminomutases in beta-amino acid biosynthesis, J. Am. Chem. Soc. 129 (2007) 15744.
[34] S. Pilbák, Ö. Farkas, L. Poppe, Mechanism of the tyrosine ammonia lyase reaction-tandem nucleophilic and electrophilic enhancement by a proton transfer, Chem. Eur. J. 18 (2012) 7793–7802.
[35] S. Bartsch, U.T. Bornscheuer, A single residue influences the reaction mechanism of ammonia lyases and mutases, Angew. Chem. Int. Ed. 48 (2009) 3362–3365.
[36] O. Amata, T. Marino, N. Russo, M. Toscano, A proposal for mitochondrial processing peptidase catalytic mechanism, J. Am. Chem. Soc. 133 (2011) 17824–17831.
[37] M.A. Khan, R. Lo, T. Bandyopadhyay, B. Ganguly, Probing the reactivation process of sarin-inhibited acetylcholinesterase with α-nucleophiles: hydroxylamine anion is predicted to be a better antidote with DFT calculations, J. Mol. Graphics Modell. 29 (2011) 1039–1046.
[38] X. Sheng, Y.J. Liu, C.B. Liu, Theoretical studies on the common catalytic mechanism of transketolase by using simplified models, J. Mol. Graphics Modell. 39 (2013) 23–28.
[39] S.L. Chen, W.H. Fang, F. Himo, Theoretical study of the phosphotriesterase reaction mechanism, J. Phys. Chem. B 111 (2007) 1253–1255.
[40] E.F. Oliveira, N.M.F.S.A. Cerqueira, P.A. Fernandes, M.J. Ramos, Mechanism of formation of the internal aldimine in pyridoxal 5′-phosphate dependent enzymes, J. Am. Chem. Soc. 133 (2011) 15496–15505.
[41] H.M. Senn, W. Thiel, QM/MM methods for biomolecular systems, Angew. Chem. Int. Ed. 48 (2009) 1198–1229.
[42] P. Hu, Y.K. Zhang, Catalytic mechanism and product specificity of the histone lysine methyltransferase SET7/9. An ab initio QM/MM-FE study with multiple initial structures, J. Am. Chem. Soc. 128 (2006) 1272–1278.
[43] Q.Q. Hou, L.K. Du, J. Gao, Y.J. Liu, C.B. Liu, QM/MM study on the reaction mechanism of O6-alkylguanine-DNA alkyltransferase, J. Phys. Chem. B 114 (2010) 15296–15300.
[44] C. Lee, W. Yang, R.G. Parr, Development of the colle-salvetti of the electron density, Phys. Rev. B: Condens. Matter 37 (1988) 785–789.
[45] A.D. Becke, Density-functional exchange-energy approximation with correct asymptotic behavior, Phys. Rev. A 38 (1988) 3098–3100.
[46] A.D. Becke, Density-functional thermochemistry I. The effect of the exchange-only gradient correction, J. Chem. Phys. 96 (1992) 2155–2160.
[47] A.D. Becke, Density-functional thermochemistry. II. The effect of the Perdew-Wang generalized-gradient correlation correction, J. Chem. Phys. 97 (1992) 9173–9177.
[48] A.D. Becke, Density-functional thermochemistry. III. The role of exact exchange, J. Chem. Phys. 98 (1993) 5648–5652.
[49] M. Frisch, et al., GAUSSIAN 03 Revision D. 01, Gaussian Inc., Wallingford, CT, 2004.
[50] S. Miertuš, E. Scrocco, J. Tomasi, Electrostatic interaction of a solute with a continuum. A direct utilizaion of ab initio molecular potentials for the prevision of solvent effects, Chem. Phys. 55 (1981) 117–129.
[51] R. Cammi, J. Tomasi, The GEPOL-GB method for cavity construction, J. Comput. Chem. 16 (1995) 1449–1458.
[52] G.M. Morris, D.S. Goodsell, R.S. Halliday, R. Huey, W.E. Hart, R.K. Belew, A.J. Olson, Automated docking using a Lamarckian genetic algorithm and an empirical binding free energy function, J. Comput. Chem. 19 (1998) 1639–1662.
[53] R. Stowasser, R. Hoffmann, What do the Kohn–Sham orbitals and eigenvalues mean? J. Am. Chem. Soc. 121 (1999) 3414–3420.
[54] F.M. Bickelhaupt, E.J. Baerends, W. Ravenek, Model systems for initial stages of oxidative-addition reactions. Theoretical investigation of η1 and η2 coordination of F2 and H2 to PtCl42- and Cr(CO)5, Inorg. Chem. 29 (1990) 350–354.
[55] W. Mutatu, K.L. Klettke, C. Foster, K.D. Walker, Unusual mechanism for an aminomutase rearrangement: retention of configuration at the migration termini, Biochemistry 46 (2007) 9785–9794.
[56] B. Wu, W. Szymański, G.G. Wybenga, M.M. Heberling, S. Bartsch, S. de Wildeman, G.J. Poelarends, B.L. Feringa, B.W. Dijkstra, D.B. Janssen, Mechanism-inspired engineering of phenylalanine aminomutase for enhanced β-regioselective asymmetric amination of cinnamates, Angew. Chem. Int. Ed. 51 (2012) 482–486.
[57] L. Melander, W.H. Saunders Jr., Reaction Rates of Isotopic Molecules, R.E. Krieger, Malabar, FL, 1987, Chapter 2.
[58] M.J. Knapp, K. Rickert, J.P. Klinman, Nature of hydrogen transfer in soybean lipoxygenase 1: separation of primary and secondary isotope effects, J. Am. Chem. Soc. 124 (2002) 12218–12228.
[59] J. Mavri, H. Liu, M.H.M. Olsson, A. Warshel, Simulation of tunneling in enzyme catalysis by combining a biased propagation approach and the quantum classical path method: application to lipoxygenase, J. Phys. Chem. B 112 (2008) 5950–5954.
[60] S.C.L. Kamerlin, J. Mavri, A. Warshel, Examining the case for the effect of barrier compression on tunneling, vibrationally enhanced catalysis, catalytic entropy and related issues, FEBS Lett. 584 (2010) 2759–2766.